

Articles

High-Resolution Fluorescence Near-Field Imaging of Individual Nanoparticles via the Tip-Induced Quenching Technique

Won-Hwa Park and Zee Hwan Kim*

Department of Chemistry and Center for Photo- and Electro-Responsive Molecules, Korea University, Seoul 136-701, Korea

*E-mail: zhkim@korea.ac.kr

Received September 28, 2007

We demonstrate that high-resolution (~60 nm) near-field fluorescence images of fluorescent nanospheres can be obtained by utilizing the tip-induced fluorescence quenching process. A time-stamped photon counting (TSPC) technique employed enables us to efficiently measure the degree of fluorescence quenching caused by the dielectric or metallic atomic force microscopy tip. We find that the degree of quenching is not only determined by the tip-material but also by the local morphology of the tip. The fringe patterns around individual nanospheres observed are explained in terms of the interference between the excitation field that is directly induced by the laser source, and the scattered excitation field from the tip.

Key Words : Fluorescence, Microscopy, Quenching

Introduction

The ability to optically image individual molecules and particles without ensemble averaging has benefited many different disciplines of science such as biology, chemistry, materials science, and nanoscience.¹ However, the resolving power of the conventional optical microscopy is strictly limited by the diffraction of light and the resulting spatial resolution achievable is a half of the excitation wavelength, which often prevents establishing the definite morphology-property, or structure-function relationship for nanomaterials and biomolecules. The fiber-optic based near-field scanning optical microscopy (NSOM)² partly overcomes this diffraction limit of light and allows one to map out local optical properties with a spatial resolution of ~100 nm.

The apertureless NSOM (ANSOM) uses a radically different approach to obtain higher-spatial resolution in images. In ANSOM, an externally illuminated metallic tip confines the electromagnetic field within a few tens of nanometers in size, and the confined light at the apex of the tip acts as a nano-sized light source for fluorescence,³⁻⁸ Raman,^{9,10} and Rayleigh scattering imaging.¹¹⁻¹³ Many researchers already explored the possibility for fluorescence-ANSOM (F-ANSOM, or tip-enhanced fluorescence microscopy) technique. However, it is found that the presence of the metallic tip not only enhances, but it also quenches the local fluorescence, which prevents successful realization of FANSOM adequate for general applications. These competing roles (enhancement versus quenching) of the metallic tip continue to be the focus of debate in nano-optics communities since the first report by Xie and co-workers.⁵

Here we propose a pragmatic approach for the high-resolution near-field fluorescence imaging that fully utilizes

the tip-induced fluorescence quenching. Note that both the fluorescence-enhanced or fluorescence-quenched NSOM can provide equivalent nanometer-resolution fluorescence images as long as the following two conditions are met: (1) the quenching or enhancement radius (the distance at which tip enhances or quenches the fluorescence of the nano-object) is sufficiently short (*e.g.*, a few tens of nanometers), and (2) the un-enhanced or un-quenched fluorescence background is efficiently removed from the images. However, the potential for the quenching-induced microscopy has not been explored thus far. In this work, we employ the time-stamped photon counting technique (TSPC) to measure the tip-induced fluorescence quenching of nanospheres and to reject the un-quenched fluorescence background. Our results unambiguously show that the quenching apertureless NSOM (Q-ANSOM for short) indeed provides nano-scale fluorescence images.

Experimental Setup and Photon Counting Algorithm.

The instrument employed is a custom-built inverted confocal microscope combined with a tapping-mode atomic force microscope (AFM) (Figure 1). A linearly polarized excitation light from an Ar⁺ laser (514 nm) is delivered into the entrance port of the inverted confocal microscope through a dichroic beam splitter, and focused on the sample surface by a high-numerical aperture objective lens (1.4 NA, oil-immersion type). The laser power at sample position is less than 100 mW. The same lens collects the fluorescence in epi-direction and it is spatially filtered through a 150 μm pinhole. The Rayleigh back-scattering is rejected by an emission filter placed in front of a single-photon avalanche photodiode (SPAD) detector. The AFM tips employed are etched silicon or gold-coated silicon tips purchased from Micromasch Inc.

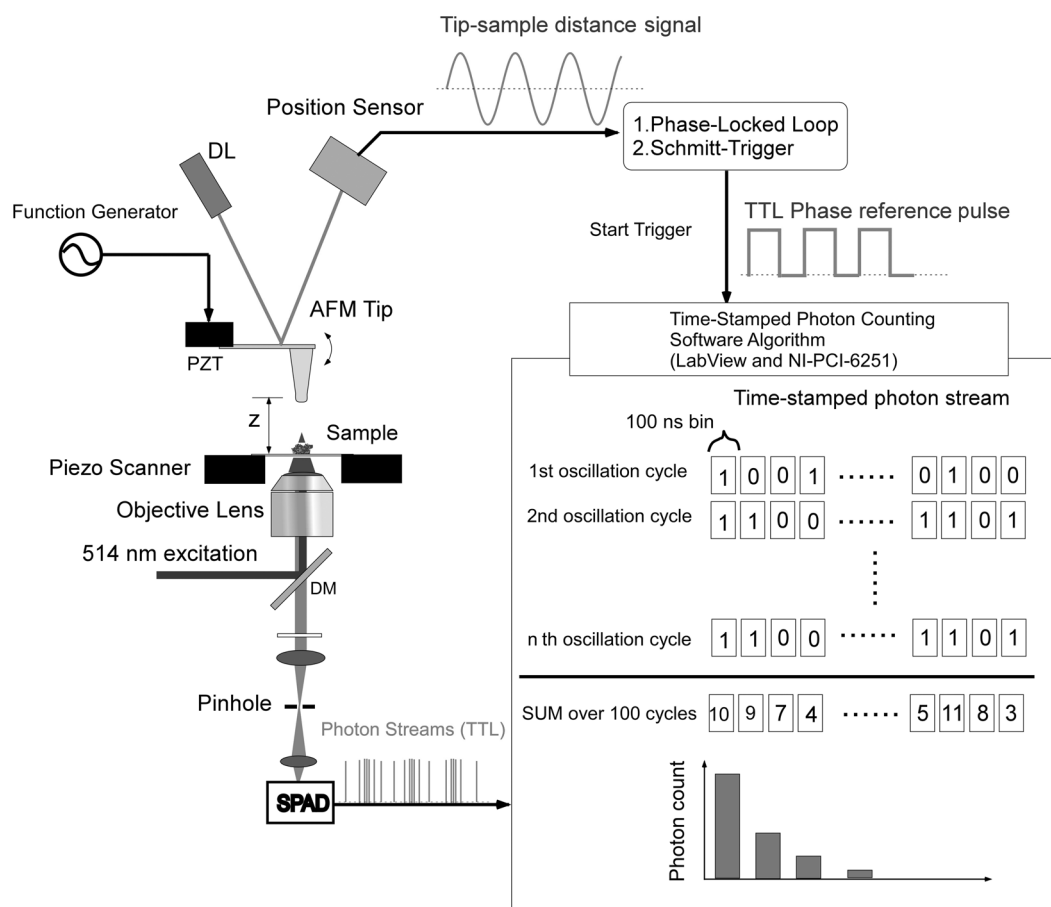


Figure 1. The schematic diagram of the microscope and the outline of photon counting algorithm. DM = dichroic mirror, DL = diode laser, SPAD = single-photon avalanche photodiode.

The photon counting algorithm we have developed is an all-digital, software based counting procedure that accumulates the number of fluorescence photons separately for different phases of oscillation of the tip. One might wonder if the well-established lock-in amplification technology could be applied to the current experiment. However, the number of fluorescence photons in our experiment is not sufficient enough to register a smooth analog wave of signal. Instead, the fluorescence photons arrive at the detector as a stream of discrete pulses. Therefore, each of the photon counting pulse (about 100 ps in width) carries broad Fourier frequency components, which are detected as a white noise in lock-in amplifier. Therefore, we have developed an alternative phase-sensitive photon-counting method that takes full advantage of tapping-mode AFM operation. The sinusoidal tapping signal from the home-built AFM head is converted to a TTL (transistor-transistor logic) wave by a combination of the Schmitt-trigger and phase-locked loop (PLL) circuits. The rising-edge of the tapping TTL pulse acts as a zero-phase reference of the tip oscillation. A stream of another TTL pulses from the SPAD (fluorescence photons) is directly fed into the input of a fast digital data-acquisition board (National Instrument, PCI-6251) operating at 20 MHz bandwidth. These two streams of TTL pulses are synchronously stored for 100-1000 tip oscillation cycles in

the data acquisition computer, and the phase-dependent photon counting histograms, $N(\phi)$, where the ϕ is the tip oscillation phase that spans $0-2\pi$ range, are accumulated. Finally, the phase-dependent photon counting histogram is converted to the distance-dependent fluorescence photon counting histogram, $N(z)$, via the relationship between the oscillation phase, ϕ , and the instantaneous tip-sample distance, z :

$$z(\phi) = A_0/2(1 + \cos \phi), \quad (1)$$

where the z is the tip-sample distance, and the A_0 is the tip oscillation amplitude. The tip-induced quenching, Q , is defined by:

$$Q = N(z_{\max}) - N(z_{\min}), \quad (2)$$

where z_{\max} and z_{\min} are the maximum and minimum tip-sample distances, respectively. Tip-induced quenching ANSOM and the AFM images are simultaneously acquired by raster-scanning the sample using a closed-loop piezo-scanner. Each pixel in Q-ANSOM images represents the quenching, Q , induced by the dielectric or metallic AFM tip, as defined in eqn (2). The samples we used were the commercially available CdSe/ZnS quantum dots (Invitrogen Inc, 11 nm diameter, core diameter ~ 4 nm) and dye-doped polystyrene nanospheres (~ 40 nm) spin-cast onto the

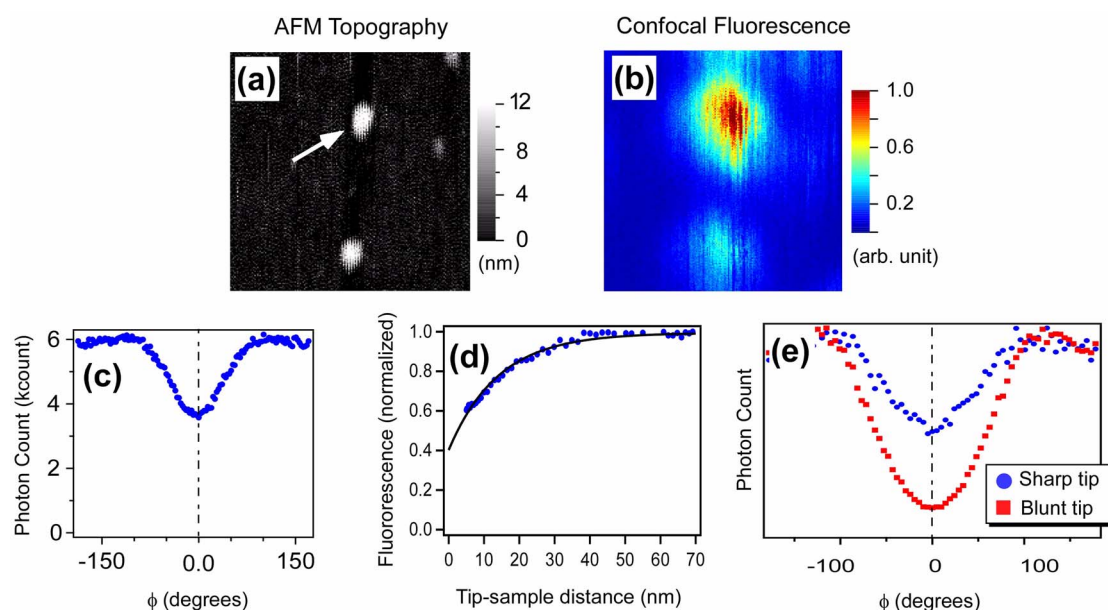


Figure 2. The (a) AFM topography and (b) confocal fluorescence of CdSe/ZnS quantum dots obtained simultaneously ($2 \mu\text{m} \times 2 \mu\text{m}$). (c) Fluorescence intensity as a function of tip oscillation phase obtained at the position marked in (a). The zero-phase of the oscillation is set at minimum tip-sample vertical distance (z_{min}). (d) Fluorescence intensity (filled circles) as a function of tip-sample distance, derived from (c). The x-axis is displaced by 5 nm to take into account the thickness of the polymer coating on CdSe/ZnS nanoparticle. Also shown in solid line is the fit to the *ad hoc* equation, $y = a(1 - b \exp(-(z - z_0)/c))$, which gives characteristic quenching distance of $c = 14$ nm. (e) Fluorescence versus tip oscillation phase obtained above a dye-doped polystyrene nanosphere, obtained with a gold coated tip with sharp (solid circles) and blunt tip (solid squares) morphologies.

cleaned glass cover-slip.

Results and Discussion

Figures 2a and 2b display the conventional confocal fluorescence and AFM topography images of two isolated CdSe/ZnS nanoparticles. The confocal images show nearly diffraction limited resolution of ~ 200 nm. Figure 2c is the fluorescence photon counting histogram as a function of the Si-tip oscillation phase, while the tip positioned directly above a CdSe/ZnS nanoparticle (marked in Figure 2b). In this Figure, the $\phi = 0^\circ$ and 180° position correspond to the minimum (tip in-contact with the particle), and maximum (tip away from the particle) tip-sample distances, respectively. Figure 2d shows the plot of fluorescence intensity as a function of tip-sample distance, as derived from the phase-dependent photon counting histogram shown in Figure 2c. We do not find any signature of the tip-enhanced fluorescence. Instead, we observe a significant quenching induced by the tip. As can be seen from the Figures 2c and 2d, the fluorescence from the quantum dot is not completely quenched on contact with Si-tip (the fluorescence intensity is not zero with $z = z_{\text{min}}$), which is caused by the thick polymer coating (about 5 nm thickness) on the CdSe/ZnS quantum dots. We find that the decay length of the fluorescence is about 14 nm, which is significantly larger than the usual Förster quenching radius of < 5 nm. It is important to note that the dielectric or metallic surface-induced quenching has completely different mechanism from the usual Förster- or Dexter-type resonant energy transfer processes. The mirror

(surface) placed closely to a dipole emitter (a single nanoparticle or a molecule) generates a mirror image of the emitting dipole at the conjugate position of the real dipole. These two dipoles oscillate out of phase and reduce (quench) overall fluorescence efficiency.¹⁴ Based on this dipole-image dipole interaction picture, we expect that the characteristic quenching length of a few tens of nanometers is mostly determined by the dielectric constants of the surfaces.¹⁵ However, we find that the degree of quenching is also affected by the detailed morphology of the tips as well as the materials of the tip. Figure 2e shows one such example. In this figure, we compare the fluorescence quenching curves of a dye-doped polystyrene nanosphere, obtained with a sharp gold-coated tip and a blunt gold-coated tip. We find that blunt tips induce stronger quenching than the sharp ones. At this point, we are unable to provide a definite explanation for the tip-morphology dependent quenching efficiencies. Nevertheless, our data does show that the tip does not merely acts as a locally flat mirror in inducing the fluorescence quenching. Instead, local irregularities and/or the sharpness of the metallic surfaces must play a role in determining the fluorescence quenching efficiencies. Overall, the surface-induced quenching distance of ~ 10 nm sets the ultimate spatial resolution achievable with tip-induced quenching ANSOM images, as will be described in the below.

Figure 3 presents the AFM, confocal, and quenching ANSOM (Q-ANSOM) images of dye-doped polystyrene nanoparticles obtained with a gold coated tip. The polystyrene nanospheres (diameter 40 nm) appear as spherical dots of ~ 60 nm widths in the AFM images because of the

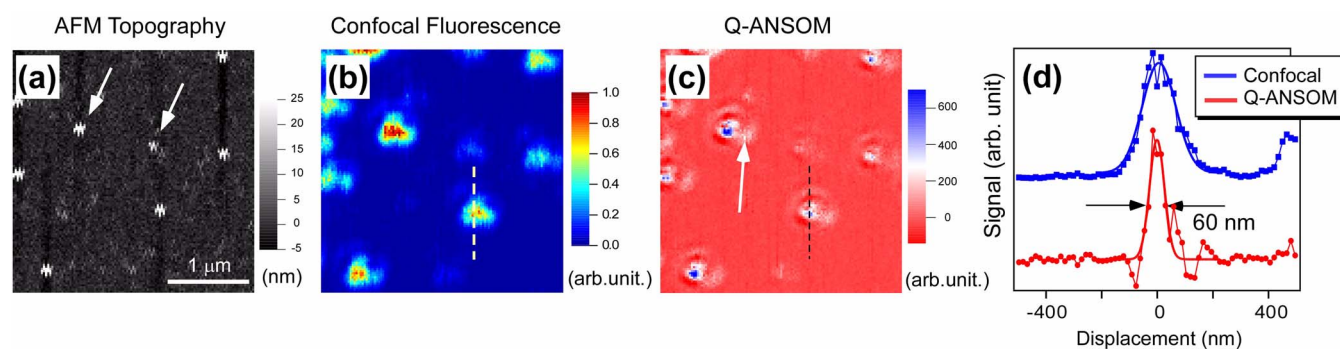


Figure 3. The (a) AFM topography, (b) confocal fluorescence, and (c) Q-ANSOM images of dye-doped polystyrene nanospheres obtained simultaneously ($3 \mu\text{m} \times 3 \mu\text{m}$). The arrows in (a) indicate two nanospheres with significantly different fluorescence intensities (see text). The arrow in (c) indicates the fringe structure mentioned in the text. (d) Comparison of the line profiles of confocal (blue squares) and Q-ANSOM (red circles) images marked in (b) and (c) in dashed lines. Also shown are the Gaussian fit of the profiles (solid lines) and the width of the Q-ANSOM profile.

tip-convolution effect. The confocal fluorescence images exhibit near-diffraction limited spot size of FWHM ~ 200 nm. The confocal spots in our image do not have perfectly circular Airy's disc structures, because of the wave-front distortion induced by the metallic tip present close to the nanosphere.

The Q-ANSOM images are obtained by accumulating the phase-dependent photon counting histogram ($N(\phi)$) similar to the one shown in Figures 2c and 2e, and evaluating the fluorescence intensity difference between the photon counting at $\phi = 0^\circ$ (tip in contact with the sample) and at $\phi = 180^\circ$ (tip away from the sample) for each sample positions. Bright spots in our quenching image correspond to the regions with significant quenching occurs. As can be clearly seen from the Figure 3c, the Q-ANSOM image shows fluorescence map of nanospheres with a spatial resolution (~ 60 nm) significantly better than the diffraction limit. Moreover, the Q-ANSOM shows significantly different intensities for two nanospheres (arrows in Figure 3a) with similar in size, which confirms that the Q-ANSOM is a genuine optical images, not the artifact derived from the sample topography.¹⁶ The Figure 3d compares the line profiles of the confocal and Q-ANSOM images shown in Figures 3b and 3c, which shows ~ 60 nm spatial resolution of Q-ANSOM. Currently, our estimate of the spatial resolution is limited by the finite size of the nanospheres (40 nm) also by the sharpness of the metallic tip (radius of curvature ~ 70 nm). Therefore, actual spatial resolution is likely to be better than 60 nm.

Upon closer examination of the Q-ANSOM images, we find that our images not only show intense quenching spots, but they also show fringe patterns around each nanosphere positions (Figure 4). The fringe pattern is not likely originated from the fluorescent nanosphere itself, because of the incoherent nature of the fluorescence photons generated by an ensemble of dye molecules that are embedded in polystyrene nanospheres. Instead, we believe that the fringe structure originates from the interference between the two illumination-paths of the nanosphere: the nanosphere can be (1) directly illuminated by the light source, and also (2)

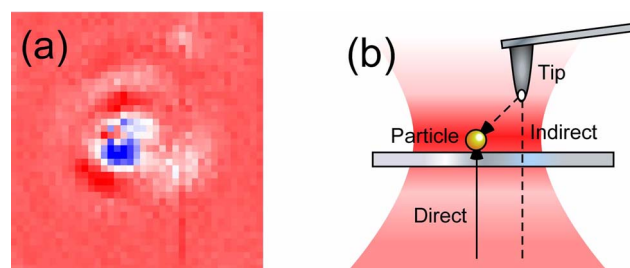


Figure 4. (a) The sample fringe structure of Q-ANSOM around a nanosphere ($1 \mu\text{m} \times 1 \mu\text{m}$). (b) Proposed mechanism of the interference fringe pattern generation in Q-ANSOM images.

indirectly illuminated via the scattered light from the tip (see Figure 4). The scanning of the tip modulates the relative phases of the direct and indirect illumination paths, and constructive and destructive interference between these two excitation paths lead to the stronger and weaker fluorescence from the nanospheres. We also observe a slight azimuthal asymmetry of the fringe (see Figure 4). At this point, we are unable to provide a definite answer to this asymmetry. We speculate that the asymmetric fringe may originate from uneven wave-front of the excitation beam, asymmetric scattering from the tip-apex, or the finer-structures of the nanosphere.

Conclusion

In this work, we have demonstrated that tip-induced fluorescence quenching microscopy can reveal high-resolution (~ 60 nm) fluorescence images of individual fluorescent nanospheres. In addition, we find that the degree of quenching is not only determined by the tip-material but also by the local morphology of the tip. The fringe patterns around a single nanosphere observed are explained in terms of the excitation beam interference effect. One of the major advantages of the Q-ANSOM over the fluorescence-enhanced ANSOM is the insensitivity toward the nano-optical or plasmonic character of the tip itself. The tip-enhanced fluorescence microscopy critically relies on the plasmon

resonant excitation of the tip-field, which requires careful fine-tuning of the nano-optical properties of the tip (e.g., materials, excitation wavelength, and the nanometric shapes). On the other hand, the tip-induced quenching occurs both with the dielectric or metallic tip independent of the plasmonic character of the tip. Current experiment involves only one kinds of fluorophore and the fluorescence emission is detected without any wavelength selectivity. We believe that a fully multiplexed Q-ANSOM that can simultaneously image several kinds of fluorophores based on different fluorescence wavelengths should greatly benefit the colocalization studies in biological processes.

Acknowledgments. This work was supported by the Ministry of Science and Technology (MOST) grant funded by the Korean government (MOST) (No. RH0-2005-000-01004-0, 2007). W.-H. Park thanks Seoul Metropolitan government for the Seoul Science Fellowship.

References

1. Moerner, W. E.; Orrit, M. *Science* **1999**, 283(5408), 1670.
 2. Paesler, M. A.; Moyer, P. J. *NEAR-FIELD OPTICS: THEORY, INSTRUMENTATION, AND APPLICATION*, 1st ed.; John Wiley & Sons: New York, 1996.
 3. Ziyang, M.; Jordan, M. G.; Lawrence, A. W.; Stephen, R. Q. *Phys. Rev. Lett.* **2006**, 97(26), 260801.
 4. Sergei, K.; Ulf, H.; Lavinia, R.; Vahid, S. *Phys. Rev. Lett.* **2006**, 97(1), 017402.
 5. Sanchez, E. J.; Novotny, L.; Xie, X. S. *Phys. Rev. Lett.* **1999**, 82(20), 4014.
 6. Pascal, A.; Palash, B.; Lukas, N. *Phys. Rev. Lett.* **2006**, 96(11), 113002.
 7. Kramer, A.; Trabesinger, W.; Hecht, B.; Wild, U. P. *Appl. Phys. Lett.* **2002**, 80(9), 1652.
 8. Jordan, M. G.; Lawrence, A. W.; Guillaume, A. L.; Ma, Z.; Stephen, R. Q. *Phys. Rev. Lett.* **2004**, 93(18), 180801.
 9. Stockle, R. M.; Suh, Y. D.; Deckert, V.; Zenobi, R. *Chem. Phys. Lett.* **2000**, 318(1-3), 131.
 10. Anderson, N.; Hartschuh, A.; Cronin, S.; Novotny, L. *J. Am. Chem. Soc.* **2005**, 127(8), 2533.
 11. Knoll, B.; Keilmann, F. *Opt. Commun.* **2000**, 182(4-6), 321.
 12. Knoll, B.; Keilmann, F. *Nature* **1999**, 399(6732), 134.
 13. Hillenbrand, R.; Keilmann, F. *Phys. Rev. Lett.* **2000**, 85(14), 3029.
 14. Ohtsu, M.; Kobayashi, K. *Optical Near Fields*; Springer-Verlag: Berlin, 2004.
 15. Ebenstein, Y.; Yoskovitz, E.; Costi, R.; Aharoni, A.; Banin, U. *J. Phys. Chem. A* **2006**, 110(27), 8297.
 16. Hecht, B.; Bielefeldt, H.; Inouye, Y.; Pohl, D. W.; Novotny, L. *J. Appl. Phys.* **1997**, 81(6), 2492.
-